coatings

MDPI

Article

Using an Atmospheric Pressure Chemical Vapor Deposition Process for the Development of V_2O_5 as an Electrochromic Material

Dimitra Vernardou

Center of Materials Technology and Photonics, School of Applied Technology, Technological Educational Institute of Crete, 710 04 Heraklion, Crete, Greece; dimitra@iesl.forth.gr; Tel.: +30-281-037-9774

Academic Editors: Mingheng Li and Alessandro Lavacchi
Received: 11 November 2016; Accepted: 5 February 2017; Published: 8 February 2017

Abstract: Vanadium pentoxide coatings were grown by atmospheric pressure chemical vapor deposition varying the gas precursor ratio (vanadium (IV) chloride:water) and the substrate temperature. All samples were characterized by X-ray diffraction, Raman spectroscopy, scanning electron microscopy, cyclic voltammetry, and transmittance measurements. The water flow rate was found to affect the crystallinity and the morphological characteristics of vanadium pentoxide. Dense stacks of long grains of crystalline oxide are formed at the highest amount of water utilized for a substrate temperature of 450 °C. Accordingly, it was indicated that for higher temperatures and a constant gas precursor ratio of 1:7, the surface morphology becomes flattened, and columnar grains of uniform size and shape are indicated, keeping the high crystalline quality of the material. Hence, it was possible to define a frame of operating parameters wherein single-phase vanadium pentoxide may be reliably expected, including a gas precursor ratio of 1:7 with a substrate temperature of >450 °C. The as-grown vanadium pentoxide at 550 °C for a gas precursor ratio of 1:7 presented the best electrochemical performance, including a diffusion coefficient of 9.19×10^{-11} $cm^2 \cdot s^{-1}$, a charge density of 3.1 $mC \cdot cm^{-2}$, and a coloration efficiency of 336 $cm^2 \cdot C^{-1}$. One may then say that this route can be important for the growth of large-scale electrodes with good performance for electrochromic devices.

Keywords: atmospheric pressure chemical vapor deposition (APCVD); vanadium pentoxide; electroactive material

1. Introduction

A lot of attention is given to materials that can be used in "smart windows". Responsive materials can regulate a more comfortable living environment, while saving energy usually consumed for appropriate lighting or air conditioning [1]. A typical example is the electrochromic device, which shows reversible optical changes in response to an applied voltage. One of the most studied cathodes for electrochromic devices is vanadium pentoxide (V_2O_5) [2–5]. A foreign atom such as Li^+ can be intercalated or deintercalated from its lattice, switching reversibly from a bleached to a colored state through the following reaction [6]:

$$\text{(bleached) } V_2O_5 + xLi^+ + xe^- \text{ <=> } Li_xV_2O_5 \text{ (colored)}$$

V_2O_5 is the only oxide that can show both anodic and cathodic coloration [7]. The reversible Li^+ intercalation/deintercalation processes of V_2O_5 lead to both reversible optical and multicolor changes for aesthetics in the voltage range ±1 V [8–10].

Electrochromic V_2O_5 coatings have been prepared by electrodeposition [11,12], "Doctor Blade" [13], reactive sputtering [14], polyol process [15], sol–gel [16], and hydrothermal growth [17]. Strategies

based on solution can hardly be up-scaled, due to the long reaction period, toxic reducing agents, and large amount of solvent required. Additionally, methods such as sputtering are not compatible with on-line manufacture. Hence, a low-cost, simple, and easily integrated into float-glass production lines technique is required.

As with many coatings, chemical vapor deposition (CVD) routes are more attractive for the production of vanadium oxides on glass than other conventional techniques, since the stoichiometry and the morphology of the coatings can be simply controlled by tuning the vapor flows in the coating zone [18,19]. In addition, the simplicity of CVD—particularly when performed at atmospheric pressure (APCVD)—makes such a process compatible with on-line glass manufacturing processes. Nevertheless, there are very few reports related to APCVD electrochromic V_2O_5 [18].

The aim of this work is to define a frame of APCVD operating parameters wherein single-phase V_2O_5 may be reliably expected to form. Additionally, a correlation of the morphological characteristics with the corresponding electrochemical/electrochromic performance of the coatings is highlighted, which is important for the understanding and the enhancement of Li^+ intercalation into the vanadium oxide matrix.

2. Materials and Methods

The APCVD reactor used in this work is an in-house design, and consists of a cold-wall reactor connected to an arrangement of stainless-steel heated pipes, valves, and bubblers, as shown in Figure 1 [18]. Bubbler 1 was used for the vanadium (IV) chloride, VCl_4 (Aldrich, Munich, Germany, 99%), and bubbler 2 for the deionised H_2O. The carrier gas was N_2, which was passed through the apparatus during all operations of the reactor. During the growth, two series of experiments were performed varying the precursor ratio of VCl_4:H_2O (1:1, 1:2, 1:3, 1:5, and 1:7) at 450 °C and the substrate temperature (500 and 550 °C) for constant ratio of VCl_4:H_2O, 1:7. The deposition time was 2 min. The substrates used during the APCVD experiments were commercial fluorine-doped SnO_2 (FTO)-precoated glass substrates (Pilkington, Manchester, UK), all of dimensions 2 cm × 2 cm × 0.3 cm. Prior to coating, all substrates were cleaned with H_2O and detergent, rinsed thoroughly with H_2O and deionised H_2O, and allowed to dry.

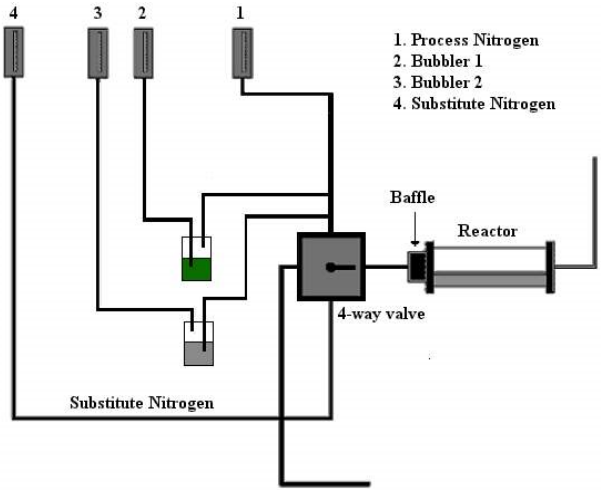

Figure 1. A schematic presentation of the atmospheric pressure chemical vapor deposition (APCVD) reactor.

X-ray diffraction (XRD) measurements were carried out in a Siemens D5000 Diffractometer (SCIMED, Manchester, UK) for 2-θ = 10.00°–60.00°, step-size = 0.02°, and step time = 30 s/°. Raman measurements were performed with a Nicolet Almega XR micro-Raman system (CRAIC, Hertfordshire, UK) operating at wavenumber range of 100–1100 cm^{-1} using a 473 nm laser. Scanning electron

microscopy (SEM) was utilized for the morphology observation of the as-grown coatings through a Jeol JSM-6390LV electron microscope (JEOL, Freising, Germany). For the SEM characterization, all samples were over-coated with a thin film of gold to make them more conductive. UV-Vis transmittance spectra were obtained using a Perkin Elmer Lambda 950 spectrometer over the wavelength range of 300–1100 nm. Finally, cyclic voltammetry experiments were performed using an electrochemical cell with a tri-electrode configuration and a computer-controlled AUTOLAB potentiostat/galvanostat [19–23]. Vanadium oxide-coated glass substrates acted as the working electrode biased in the range between −1 and +1 V. Ag/AgCl and a Pt foil were employed as the reference and the counter electrode, respectively. Additionally, cyclic voltammograms were obtained at scan rates of 2, 5, 10, 20, 30, 40, 50, 75, 100, 150, and 200 $mV \cdot s^{-1}$. To study Li^+ intercalation/deintercalation process with respect to time, chronoamperometry for a step of 200 s was carried out at −1 and +1 V. In all cases, the electrolyte was 1 M, $LiClO_4$/polypropylene carbonate.

Finally, the coating's thickness was estimated using a profilometer A-step TENCOR (KLA Tencor, Dublin, Ireland) by etching the vanadium oxide coatings off the FTO glass substrate in 1:3 H_2O_2 (30%):HCl. FTO remained intact, and the thickness was deduced from the measured step height.

3. Results and Discussion

The coatings produced in the APCVD reaction of VCl_4 and deionised H_2O were yellow, adhesive, and they passed the Scotch tape test. Additionally, they had similar properties (structural, morphological, optical, and electrochemical) after approximately six months, indicating their stability with time.

3.1. Structure

Figure 2 shows a representative XRD pattern of the as-grown APCVD coatings. It exhibits characteristic 2-θ values of 13.5°, 20.5°, 26.6°, 30.3°, 41.2°, and 54.8° with respective Miller indices (200), (001), (110), (301), (002), and (021), which are consistent with crystalline V_2O_5 [24].

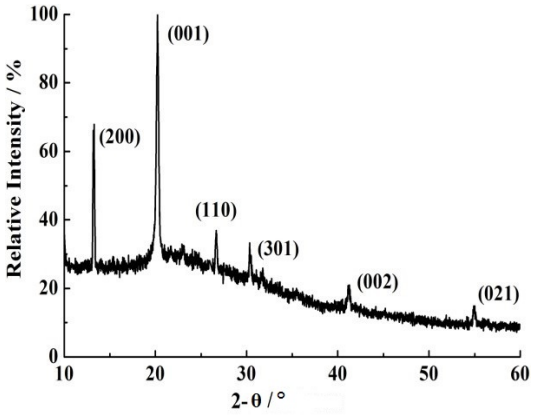

Figure 2. XRD pattern of as-grown vanadium oxide thin films by APCVD on fluorine-doped SnO_2 (FTO) glass substrates at 450 °C, using gas precursor ratio of 1:3.

Figure 3 displays the Raman spectra of V_2O_5 coatings deposited on FTO glass substrates for gas precursor ratio of VCl_4:H_2O 1:7 at 450, 500, and 550 °C. The peak positions agree with the literature spectra to within ±2 cm^{-1}. The high-frequency Raman peak at 995 cm^{-1} corresponds to the terminal oxygen (V=O) stretching mode, which results from unshared oxygen [25]. Peaks at 530 and 705 cm^{-1} are attributed to stretching modes of the V–O–V bridging bonds, with the bending motions of these bonds assigned to 486 cm^{-1} [26]. Peaks located at 283 and 406 cm^{-1} are assigned to the bending vibrations of V=O bonds [27]. Two more low-frequency Raman peaks at 145 and 197 cm^{-1} can also be distinguished, which correspond to the lattice vibrations [28].

Such outcomes suggest that by manipulating the substrate temperature, one can synthesize V_2O_5 with some oxygen deficiency. This happens because the high temperature (>450 °C) enhances the surface mobility and the crystallization due to highly reactive atomic and anionic oxygen, which can act as crystallization agents towards the composition of V_2O_5 [29]. Additionally, XRD analysis gave no indication of oxygen deficiency, but Raman study revealed the presence of additional peaks along with those of V_2O_5 at the lowest substrate temperature. This is due to the sensitivity of Raman spectroscopy to short-range vibrational modes of bond configurations, while XRD responds to long-range order crystallinity of materials [30]. Hence, the observed behavior suggests that the samples are mainly V_2O_5 retaining, however, a short-range oxygen deficiency that degrades as the substrate temperature increases.

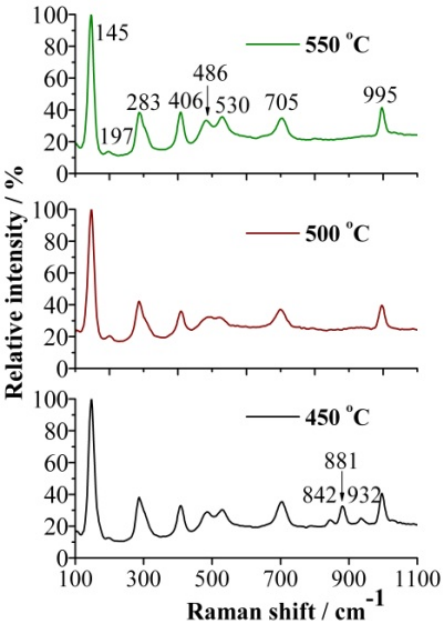

Figure 3. Raman spectra of as-grown vanadium oxide films by APCVD for a deposition time of 2 min and gas precursor ratio of VCl_4:H_2O of 1:7 at 450, 500, and 550 °C.

From the above, it is possible to define a frame of APCVD operating parameters wherein single-phase V_2O_5 may be reliably expected to form: these conditions involve a precursor ratio equal to 1:7, with a substrate temperature of >450 °C. This observation contradicts previous studies [31] due to the different designs of APCVD reactors utilized, the size of the substrates, the total gas flow rates (on the order of 1.5 L·min^{-1} in previous work [31], while in the present study it was 12 L·min^{-1}), and the precursor delivery systems employed. These parameters are expected to directly influence the nature and extent of the reaction between the precursors.

3.2. Morphology

SEM images of vanadium oxide coatings deposited at 450 °C for gas precursor ratios of VCl_4:H_2O being 1:1, 1:5, and 1:7 are shown in Figure 4. As the gas precursor ratio increases to 1:7, dense stacks of long grains are formed. This behavior may originate from the mobility of species on the developing coating surface promoted by the increased H_2O ratio.

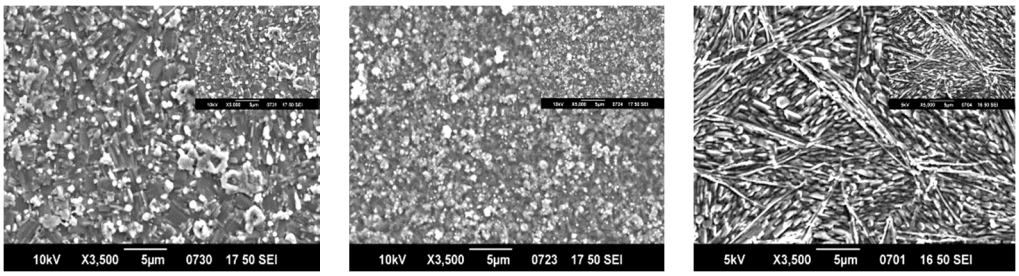

(**a**) (**b**) (**c**)

Figure 4. SEM images of the as-grown vanadium oxide coatings by APCVD at 450 °C for gas precursor ratios of VCl_4:H_2O of (**a**) 1:1, (**b**) 1:5, and(**c**) 1:7.

As the growth temperature increases from 450 to 550 °C (Figure 5), surface diffusion is activated, the surface morphology becomes flattened, and columnar grains of uniform size and shape are formed.

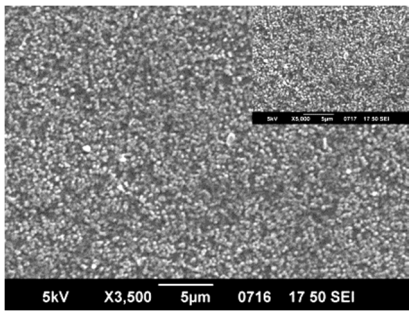

Figure 5. SEM images of the as-grown vanadium oxide coating by APCVD at 550 °C for gas precursor ratio VCl_4:H_2O of 1:7.

The growth rate of the as-grown coatings was estimated from the deposition time and the coating's thickness as derived from the profilometer. The highest value was 80 nm·min^{-1} for the deposited V_2O_5 at 550 °C. As the substrate temperature decreased to 450 °C, the growth rate was calculated to be 35 nm·min^{-1}. A proportional relationship was also seen between the amount of H_2O and the growth rate, having a maximum value of 72 nm·min^{-1} for the excess amount of H_2O introduced into the reactor (the growth rate was 15 nm·min^{-1} for the lowest amount of H_2O).

Considering these outcomes and the surface morphology of the samples, it may be suggested that either a film decomposition [32] or precursor pre-reaction with the oxygen source [33] takes place to some extent, such that the concentration of the precursor is depleted before it reaches the substrate. Since film decomposition does not occur, it is suggested that a depletion of the gas phase concentration of VCl_4 with the corresponding reduction in growth rate occurs.

3.3. Electrochemical Performance

3.3.1. Cyclic Voltammetry

The effect of substrate temperature for a constant gas precursor ratio VCl_4:H_2O of 1:7 on the electrochemical performance of the as-grown coatings was evaluated by cyclic voltammetry, as indicated in Figure 6. The potential range was −1 to +1 V at a scan rate of 10 mV·s^{-1}. All curves were normalized to the area of the working electrode, resulting in units of A·cm^{-2}. It can be observed that they all consist of four redox peaks centered at −0.19 V/+0.35 V and −0.71 V/−0.05 V (vs. Ag/AgCl), which can be assigned to the reversible Li^+ intercalation/deintercalation reaction. Initially, the coatings had a yellow color when they were cathodically polarized in $LiClO_4$, which became green and then blue with increasing cathodic potential. Then, the blue layers turned yellow again when anodically

polarized. Additionally, it becomes evident from Figure 6 that the current density of the as-grown coating at 550 °C is the highest of all, presenting an enhanced electrochemical activity. One may then suggest that the amount of incorporated charge is enhanced by the increased crystalline quality and the visibly empty space between the columnar grains rather than those left by the stacks of long grains at lower temperature. Regarding the as-grown coatings at 450 °C for gas precursor ratios of VCl_4:H_2O being 1:1, 1:2, 1:3, and 1:5, the current density was four degrees of magnitude (maximum current density of 0.000001 mA·cm^{-2}) lower than the one for 1:7, due to the immediate detachment of the oxide by the electrolyte (the working electrode was optically the same with the substrate prior to deposition). Since the electrochemical cell is made up of glass, these changes could be observed during the electrochemical measurements.

The maximum current density obtained for the as-grown coating at 550 °C (Figure 6) was lower than the colloidal crystal-assisted electrodeposited amorphous three-dimensional ordered macroporous (0.5 mA·cm^{-2} [4]), sol–gel (0.6 mA·cm^{-2} [16]), aerosol-assisted CVD (1.5 mA·cm^{-2} [34]) V_2O_5, and was comparable with APCVD (0.01 mA·cm^{-2} [18]) and hydrothermal growth (0.05 mA·cm^{-2} [17]) of V_2O_5. This value was also lower than the one obtained from the vacuum deposited (0.6 mA·cm^{-2} [35]) tungsten trioxide (WO_3), and comparable with APCVD (0.02 mA·cm^{-2} [36]), evaporation-induced self-assembly (0.06 mA·cm^{-2} [37]), low-pressure CVD (0.08 mA·cm^{-2} [38]), and hydrothermal (0.04 mA·cm^{-2} [39]) growth WO_3. Overall, this APCVD route is advantageous, since it produces higher current density compared with growth techniques which require longer reaction periods and higher substrate temperatures. On the other hand, for the cases where the current density is higher than the one reported in this work, templates and more complicated equipment are required, restricting their compatibility for large-scale manufacturing.

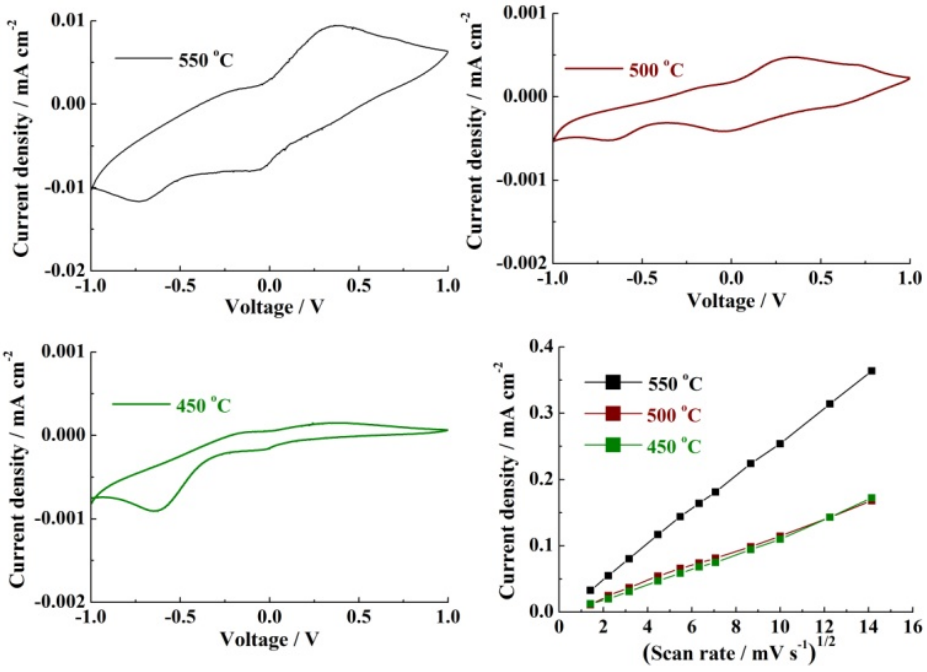

Figure 6. Cyclic voltammograms of APCVD V_2O_5 at 450, 500, and 550 °C recorded at 10 mV·s^{-1} and anodic peak current density as a function of the square root of the scan rates.

Figure 6 shows the dependence of the anodic peak current density on the square route of the scan rate, indicating a diffusion-controlled process. The diffusion coefficient of Li^+ can be obtained according to the following equations [40]:

$$I_p = D^{1/2} 2.72 \times 10^5 n^{3/2} A C v^{1/2} \quad (1)$$

$$D^{1/2} = \frac{a}{2.72 \times 10^5 n^{3/2} AC} \quad (2)$$

where n is the number of electrons, I_p is the peak current (A), D is the diffusion coefficient ($cm^2 \cdot s^{-1}$), A is the area (cm^2), C is the concentration of Li^+ ($mol \cdot cm^{-3}$), and a is the slope obtained in Figure 6. As is expected, the Li^+ diffusion coefficient of the as-grown V_2O_5 at 550 °C is the highest (9.19×10^{-11} $cm^2 \cdot s^{-1}$), which is in accordance with the above discussion. Additionally, it is well known that the Li^+ intercalation/deintercalation response is dependent on the diffusion coefficient of the species; consequently, a large diffusion coefficient will result in a fast response [40]. The diffusion coefficient of APCVD V_2O_5 estimated in this work is higher than V_2O_5 grown by atomic layer CVD [41], solution process [42], spin-coating [43], and pulsed spray pyrolysis [44], strengthening the growth of large area electrodes by APCVD with good electrochemical performance.

3.3.2. Chronoamperometry

To calculate the amount of Li^+ interchanged between the V_2O_5 and the electrolyte, chronoamperometric measurements were performed, switching the potential between −1 V and +1 V at an interval of 200 s for a total period of 2000 s, as indicated in Figure 7. It is observed that the intercalated is lower than the deintercalated charge, indicating that Li^+ remains in the material. The deintercalated charge density was estimated to be 3.1 $mC \cdot cm^{-2}$ for the as-grown V_2O_5 by APCVD at 550 °C (Figure 7), which is the highest of all due to the larger volume of active material available (i.e., highest thickness estimated).

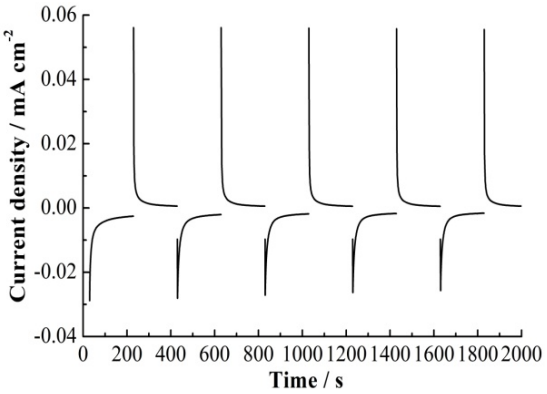

Figure 7. The chronoamperometric response at −1 and +1 V for an interval of 200 s and a total period of 2000 s of the as-grown APCVD V_2O_5 at 550 °C.

3.3.3. Ex-Situ Transmittance Measurements

The electrochromic response of the APCVD V_2O_5 at 550 °C was tested by performing transmittance measurements in the visible range and comparing the normally oxidized state at +1 V with the reduced state at −1 V, imposed by the Li^+ intercalated charge as indicated in Figure 8. It is observed that the transmittance is reduced upon cation insertion (colored state) compared to the bleached state. The contrast ratio between the two is significant, reaching a value of approximately 11 at 630 nm. Additionally, a parameter used to evaluate an electrochromic material is its coloration efficiency (CE), defined as the change in optical density (ΔOD) per unit inserted charge density ΔQ (see Equation 3 [45]),

$$CE = \frac{\Delta OD}{\Delta Q} \quad (3)$$

The CE was found to be 336 $cm^2 \cdot C^{-1}$ at 630 nm, which is one of the highest values reported if one compares it with the electrodeposited V_2O_5 (28 $cm^2 \cdot C^{-1}$ [11]), the evaporation-induced self-assembly

crystalline mesoporous WO_3 (40 $cm^2 \cdot C^{-1}$ [37]), the APCVD (≈83 $cm^2 \cdot C^{-1}$ [38]), and the vacuum deposition method of WO_3 (28 $cm^2 \cdot C^{-1}$ [35]).

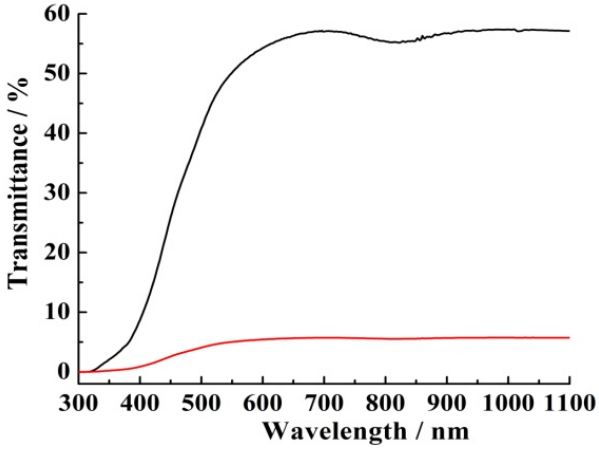

Figure 8. Transmittance spectra of APCVD V_2O_5 at 550 °C in the colored (red line) at −1 V and bleached (black line) states at +1 V.

4. Conclusions

V_2O_5 coatings were grown by APCVD, varying the gas precursor ratio of VCl_4:H_2O and the substrate temperature. From XRD and Raman spectroscopy, it was found that the samples are mainly V_2O_5, retaining, however, a short-range oxygen deficiency that degrades as the substrate temperature increases. As the amount of oxygen source introduced into the reactor increases to the maximum value, dense stacks of long grains are formed. On the contrary, the increase of substrate temperature results in surface diffusion activation, and columnar grains of uniform size and shape are formed. It was shown that the electrochemical properties of the as-grown coatings are correlated with the crystalline quality of V_2O_5, and consequently, the morphological characteristics of the samples. From the basic characterization obtained, it was possible to define a frame of APCVD operating parameters wherein single-phase V_2O_5 may be reliably expected to form: these conditions involve a precursor ratio equal to 1:7, with a substrate temperature of >450 °C. Crystalline V_2O_5 grown at 550 °C for a ratio VCl_4:H_2O of 1:7 consisting of empty space between the columnar grains was found to exhibit improved electrochemical/electrochromic performance. The diffusion coefficient was estimated to be 9.19 × 10^{-11} $cm^2 \cdot s^{-1}$, and the charge density was 3.1 $mC \cdot cm^{-2}$, with a coloration efficiency of 336 $cm^2 \cdot C^{-1}$.

Conflicts of Interest: The author declares no conflict of interest.

References

1. Brigouleix, C.; Topart, P.; Bruneton, E.; Sabary, F.; Nouhaut, G.; Campet, G. Roll-to-Roll Pulsed dc Magnetron Sputtering Deposition of WO_3 for Electrochromic Windows. *Electrochim. Acta* **2001**, *46*, 1931–1936. [CrossRef]
2. Zhai, T.; Liu, H.; Li, H.; Fang, X.; Liao, M.; Li, L.; Zhou, H.; Koide, Y.; Bando, Y.; Golberg, D. Centimeter-Long V_2O_5 Nanowires: From Synthesis to Field-Emission, Electrochemical, Electrical Transport, and Photoconductive Properties. *Adv. Mater.* **2010**, *22*, 2547–2552. [CrossRef] [PubMed]
3. Tong, Z.; Lv, H.; Zhang, X.; Yang, H.; Tian, Y.; Li, N.; Zhao, J.; Li, Y. Novel Morphology Changes from 3D Ordered Macroporous Structure to V_2O_5 Nanofiber Grassland and its Application in Electrochromism. *Sci. Rep.* **2015**, *5*, 16864. [CrossRef] [PubMed]
4. Vernardou, D. State-of-the-art of Chemically Grown Vanadium Pentoxide Nanostructures with Enhanced Electrochemical Properties. *Adv. Mater.* **2013**, *4*, 798–810.
5. Drosos, C.; Vernardou, D. Perspectives of Energy Materials Grown by APCVD. *Sol. Energy Mater. Sol. Cells* **2015**, *140*, 1–8. [CrossRef]

6. Talledo, A.; Granqvist, C.G. Electrochromic Vanadium-Pentoxide-Based Films: Structural, Electrochemical and Optical Properties. *J. Appl. Phys.* **1995**, *77*, 4655–4666. [CrossRef]
7. Li, L.; Steiner, U.; Mahajan, S. Improved Electrochromic Performance in Inverse Opal Vanadium Oxide Films. *J. Mater. Chem.* **2010**, *20*, 7131–7134. [CrossRef]
8. Scherer, M.R.J.; Li, L.; Cunha, P.M.S.; Scherman, O.A.; Steiner, U. Enhanced Electrochromism in Gyroid-Structured Vanadium Pentoxide. *Adv. Mater.* **2012**, *24*, 1217–1221. [CrossRef] [PubMed]
9. Yang, Y.; Kim, D.; Schmuki, P. Electrochromic Properties of Anodically Grown Mixed V_2O_5-TiO_2 Nanotubes. *Electrochem. Commun.* **2011**, *13*, 1021–1025. [CrossRef]
10. Chernova, N.A.; Roppolo, M.; Dillon, A.C.; Whittingham, M.S. Layered Vanadium and Molybdenum Oxides: Batteries and Electrochromics. *J. Mater. Chem.* **2009**, *19*, 2526–2552. [CrossRef]
11. He, W.; Liu, Y.; Wan, Z.; Jia, C. Electrodeposition of V_2O_5 on TiO_2 Nanorod Arrays and Their Electrochromic Properties. *RSC Adv.* **2016**, *6*, 68997–69006. [CrossRef]
12. Tong, Z.; Zhang, X.; Lv, H.; Li, N.; Qu, H.; Zhao, J.; Li, Y.; Liu, X.-Y. From Amorphous Macroporous Film to 3D Crystalline Nanorod Architecture: A New Approach to Obtain High-Performance V_2O_5 Electrochromism. *Adv. Mater. Interfaces* **2015**, *2*, 1500230. [CrossRef]
13. Mjejri, I.; Manceriu, L.M.; Gaudon, M.; Rougier, A.; Sediri, F. Nano-Vanadium Pentoxide Films for Electrochromic Displays. *Solid State Ion.* **2016**, *292*, 8–14. [CrossRef]
14. Lin, Y.-S.; Tsai, C.-W. Reactive Sputtering Deposition of V_2O_{5-z} on Flexible PET/ITO Substrates for Electrochromic Devices. *Surf. Coat. Technol.* **2008**, *202*, 5641–5645. [CrossRef]
15. Salek, G.; Bellanger, B.; Mjejri, I.; Gaudon, M.; Rougier, A. Polyol Synthesis of Ti-V_2O_5 Nanoparticles and Their Use as Electrochromic Films. *Inorg. Chem.* **2016**, *55*, 9838–9847. [CrossRef] [PubMed]
16. Ma, X.; Lu, S.; Wan, F.; Hu, M.; Wang, Q.; Zhu, Q.; Zakharova, G.S. Synthesis and Electrochromic Characterization of Graphene/V_2O_5/MoO_3 Nanocomposite Films. *ECS J. Solid State Sci. Technol.* **2016**, *5*, P572–P577. [CrossRef]
17. Vernardou, D.; Loudoudakis, D.; Spanakis, E.; Katsarakis, N.; Koudoumas, E. Electrochemical Properties of Vanadium Oxide Coatings Grown by Hydrothermal Synthesis on FTO Substrates. *New J. Chem.* **2014**, *38*, 1959–1964. [CrossRef]
18. Vernardou, D.; Paterakis, P.; Drosos, H.; Spanakis, E.; Povey, I.M.; Pemble, M.E.; Koudoumas, E.; Katsarakis, N. A Study of the Electrochemical Performance of Vanadium Oxide Thin Films Grown by Atmospheric Pressure Chemical Vapour Deposition. *Sol. Energy Mater. Sol. Cells* **2011**, *95*, 2842–2847. [CrossRef]
19. Vernardou, D.; Pemble, M.E.; Sheel, D.W. In-Situ Fourier Transform Infrared Spectroscopy Gas Phase Studies of Vanadium (IV) Oxide Coating by Atmospheric Pressure Chemical Vapour Deposition Using Vanadyl (IV) Acetylacetonate. *Thin Solid Films* **2008**, *516*, 4502–4507. [CrossRef]
20. Vernardou, D.; Pemble, M.E.; Sheel, D.W. In-Situ FTIR Studies of the Growth of Vanadium Dioxide Coatings on Glass by Atmospheric Pressure Chemical Vapour Deposition for VCl_4 and H_2O System. *Thin Solid Films* **2007**, *515*, 8768–8770. [CrossRef]
21. Vernardou, D.; Louloudakis, D.; Spanakis, E.; Katsarakis, N.; Koudoumas, E. Functional Properties of APCVD VO_2 Layers. *Int. J. Thin Films Sci. Technol.* **2015**, *4*, 187–191.
22. Vernardou, D.; Apostolopoulou, M.; Katsarakis, N.; Koudoumas, E.; Drosos, C.; Parkin, I.P. Electrochemical Properties of APCVD α-Fe_2O_3 Nanoparticles at 300 °C. *Chem. Sel.* **2016**, *1*, 2228–2234.
23. Christou, K.; Louloudakis, D.; Vernardou, D.; Savvakis, C.; Katsarakis, N.; Koudoumas, E.; Kiriakidis, G. Effect of Solution Chemistry on the Characteristics of Hydrothermally Grown WO_3 for Electroactive Applications. *Thin Solid Films* **2015**, *594*, 333–337. [CrossRef]
24. Su, Q.; Huang, C.K.; Wang, Y.; Fan, Y.C.; Lu, B.A.; Lan, W.; Wang, Y.Y.; Liu, X.Q. Formation of Vanadium Oxides with Various Morphologies by Chemical Vapor Deposition. *J. Alloys Compd.* **2009**, *475*, 518–523. [CrossRef]
25. Lee, S.-H.; Cheong, H.M.; Seong, M.J.; Liu, P.; Tracy, C.E.; Mascarenhas, A.; Pitts, J.R.; Deb, S.K. Raman Spectroscopic Studies of Amorphous Vanadium Oxide Thin Films. *Solid State Ion.* **2003**, *165*, 111–116. [CrossRef]
26. Abello, L.; Husson, E.; Repelin, Y.; Lucazeau, G. Vibrational Spectra and Valence Force Field of Crystalline V_2O_5. *Spectrochim. Acta A Mol. Spectrosc.* **1983**, *39*, 641–651. [CrossRef]

27. Julien, C.; Nazri, G.A.; Bergström, O. Raman Scattering Studies of Microcrystalline V_6O_{13}. *Phys. Status Solidi* **1997**, *201*, 319–326. [CrossRef]
28. Jehng, J.M.; Hardcastle, F.D.; Wachs, I.E. The Interaction of V_2O_5 and Nb_2O_5 with Oxide Surface. *Solid State Ion.* **1989**, *32–33*, 904–910.
29. Cvelbar, U.; Mozetic, M.; Sunkara, M.K.; Vaddiraju, S. A Method for the Rapid Synthesis of Large Quantities of Metal Oxide Nanowires at Low Temperatures. *Adv. Mater.* **2005**, *17*, 2138–2142.
30. Ocãna, M.; Garcia, J.V. Low-Temperature Nucleation of Rutile Observed by Raman Spectroscopy during Crystallization of TiO_2. *J. Am. Ceram. Soc.* **1992**, *75*, 2010–2012. [CrossRef]
31. Manning, T.D.; Parkin, I.P.; Clark, R.J.H.; Sheel, D.; Pemble, M.E.; Vernardou, D. Intelligent Window Coatings: Atmospheric Pressure Chemical Vapour Deposition of Vanadium Oxides. *J. Mater. Chem.* **2002**, *12*, 2936–2939. [CrossRef]
32. Awaluddin, A.; Pemble, M.E.; Jones, A.C.; Williams, P.A. Direct Liquid Injection MOCVD Growth of TiO_2 Films Using the Precursor Ti(mpd)(dmae)$_2$. *J. Phys. IV* **2001**, *11*. [CrossRef]
33. Crosbie, M.J.; Lane, P.A.; Wright, P.J.; Williams, D.J.; Jones, A.C.; Leedham, T.J.; Reeves, C.L.; Jones, J. Liquid Injection Metal Organic Chemical Vapour Deposition of Lead-Scandium-Tantalate Thin Films for Infrared Devices. *J. Cryst. Growth* **2000**, *219*, 390–396. [CrossRef]
34. Vernardou, D.; Louloudakis, D.; Katsarakis, N.; Koudoumas, E.; Kazadojev, I.I.; O'Brien, S.; Pemble, M.E.; Povey, I.M. Electrochemical Evaluation of Vanadium Pentoxide Coatings Grown by AACVD. *Sol. Energy Mater. Sol. Cells* **2015**, *43*, 601–605. [CrossRef]
35. Pang, Y.; Chen, Q.; Shen, X.; Tang, X.; Tang, L.; Qian, H. Size-Controlled Ag Nanoparticle Modified WO_3 Composite Films for Adjustment of Electrochromic Properties. *Thin Solid Films* **2010**, *518*, 1920–1924. [CrossRef]
36. Ivanova, T.; Gesheva, K.A.; Popkirov, G.; Ganchev, M.; Tzvetkova, E. Electrochromic Properties of Atmospheric CVD MoO_3 and MoO_3-WO_3 Films and Their Application in Electrochromic Devices. *Mater. Sci. Eng. B* **2005**, *119*, 232–239. [CrossRef]
37. Brezesinski, T.; Fattakhova Rohlfing, D.; Sallard, S.; Antonietti, M.; Smarsly, B.M. Highly Crystalline WO_3 Thin Films with Ordered 3D Mesoporosity and Improved Electrochromic Performance. *Small* **2006**, *2*, 1203–1211. [CrossRef] [PubMed]
38. Psifis, K.; Louloudakis, D.; Vernardou, D.; Spanakis, E.; Papadimitropoulos, G.; Davazoglou, D.; Katsarakis, N.; Koudoumas, E. Effect of O_2 Flow Rate on the Electrochromic Response of WO_3 Grown by LPCVD. *Phys. Status Solidi C* **2015**, *12*, 1011–1015. [CrossRef]
39. Christou, K.; Louloudakis, D.; Vernardou, D.; Katsarakis, N.; Koudoumas, E. One-Pot Synthesis of WO_3 Structures at 95 °C Using HCl. *J. Sol-Gel Sci. Technol.* **2015**, *73*, 520–526. [CrossRef]
40. Jiao, Z.; Wei Sun, X.; Wang, J.; Ke, L.; Volkan Demir, H. Hydrothermally Grown Nanostructured WO_3 Films and Their Electrochromic Characteristics. *J. Phys. D Appl. Phys.* **2010**, *43*, 285501. [CrossRef]
41. Lantelme, F.; Mantoux, A.; Groult, H.; Lincot, D. Electrochemical Study of Phase Transition Processes in Lithium Insertion in V_2O_5 Electrodes. *J. Electrochem. Soc.* **2003**, *150*, A1202–A1208. [CrossRef]
42. Watanabe, T.; Ikeda, Y.; Ono, T.; Hibino, M.; Hododa, M.; Sakai, K.; Kudo, T. Characterization of Vanadium Oxide Sol as a Starting Material for High Rate Intercalation Cathodes. *Solid State Ion.* **2002**, *151*, 313–320. [CrossRef]
43. Sahana, M.B.; Sudakar, C.; Thapa, C.; Lawes, G.; Naik, V.M.; Baird, R.J.; Auner, G.W.; Naik, R.; Padmanabhan, K.R. Electrochemical Properties of V_2O_5 Thin Films Deposited by Spin Coating. *Mater. Sci. Eng. B* **2007**, *143*, 42–50. [CrossRef]
44. Patil, C.E.; Jadhav, P.R.; Tarwal, N.L.; Deshmukh, H.P.; Karanjkard, M.M.; Patil, P.S. Electrochromic Performance of Mixed V_2O_5-MoO_3 Thin Films Synthesized by Pulsed Spray Pyrolysis Technique. *Mater. Chem. Phys.* **2011**, *126*, 711–716. [CrossRef]
45. Bathe, S.R.; Patil, P.S. Electrochromic Characteristics of Fibrous Reticulated WO_3 Thin Films Prepared by Pulsed Spray Pyrolysis Technique. *Sol. Energy Mater. Sol. Cells* **2007**, *91*, 1097–1101. [CrossRef]

© 2017 by the author; licensee MDPI, Basel, Switzerland. This article is an open access article distributed under the terms and conditions of the Creative Commons Attribution (CC BY) license (http://creativecommons.org/licenses/by/4.0/).